Optical properties of 2 at %(Ln3+) doped LiGd(WO4)2 with Ln; Eu, Er and Tm, grown by μ-pulling down technique

B. Rekik, G. Alombert-Goget, Alice Berthelot, O. Benamara, K. Lebbou

Optical properties of 2 at %(Ln^{3+}) doped $LiGd(WO_4)_2$ with Ln; Eu, Er and Tm, grown by µ- pulling Down technique

B.Rekik[1], G. Alombert-Goget[2], A.Berthelot[2], O.Benamara[2], K. Lebbou[2]
[1]Laboratory LASICOM, University Saad Dahleb Blida.1, Algeria
[2]Institut Lumière Matière, UMR5306 Université Lyon 1-CNRS, Université de Lyon 69622 Villeurbanne cedex, France

Abstract:

Spectroscopic and luminescent properties of europium (Eu), erbium (Er), thulium (Tm) doped $LiGd(WO_4)_2$ fibers crystals, present high performances for investigation in phosphorus and laser applications. We have successfully grown 2 at % Eu, Er and Tm-doped $LiGd(WO_4)_2$ singles-crystals fibers by the Micro Pulling Down (µ-PD) technique (melting point above 1115°C) using a pulling rate in the range of 0.08 – 0.15mm/min. The crystallization interface was flat, with meniscus length equal to the fiber radii. The absorption and emission spectra were measured at room temperature. The absorption and emission cross sections of the Eu^{3+} , Er^{3+}, and Tm^{3+} transitions were evaluated. For the erbium cation we register $^4S_{3/2}\rightarrow{}^4I_{15/2}$, $^2H_{11/2}\rightarrow{}^4I_{15/2}$ transitions in the visible and $^4I_{13/2}\rightarrow{}^4I_{15/2}$ in IR range. The emission spectra recorded in the visible and infrared range with fluorescence correspond to $^1G_4\rightarrow{}^3F_4$ +$^3F_2$, $^3F_3\rightarrow{}^3H_6$, $^3H_4\rightarrow{}^3H_6$, and $^1G_4\rightarrow{}^3H_5$ for the thulium, instead for the europium we have $^5D_1\rightarrow{}^7F_{1,2}$ and $^5D_0\rightarrow{}^7F_{0\text{-}1\text{-}2\text{-}3\text{-}4}$, transitions. This last one presents an excellent structural probe for investigating the local environment of Eu^{3+} dopant in $LiGd(WO_4)_2$ host. The fluorescence lifetimes associated to these intense transitions were investigated. The polarized IR and Raman spectra of $LiGd(WO_4)_2$ single crystal fiber were measured, ~~according to the directions~~ parallel and perpendicular to the fibers growth direction. We observed a bonds at 915 cm^{-1} for IR and 913 cm^{-1} for Raman corresponding of the symmetric stretching mode of the isolated tetrahedra $(WO_4)^{-2}$ group.

Keywords: Double tungstate (DT); Asymmetry factor of luminescence; µ-PD; Fibers Crystal; Spectroscopy ; Three-level laser.

1. Introduction

Tungstate crystals with the general formula $A(RE)(WO_4)_2$, where A is the alkaline element ; K, Li, Na, Cs and Rb; the (RE) is trivalent element such rares earth have attracted a great attention, for their great optical properties and high performance for many applications, such as optical fibers [1], scintillator materials [2], humidity sensors [3], catalysis [4], phosphor's and laser's light, [5-12]. Furthermore, their tetragonal scheelite ($CaWO_4$) type structure provides them an excellent physical and chemical properties [13]. These materials present high chemical stability [14], high transparency in visible, and a high efficiency of luminescence because of the high absorption cross sections presented by Tungstates [15]. The $LiGd(WO_4)_2$ material crystallizes in the tetragonal structure with space symmetry group I4(1)/a (C_{4h}^6) and cell parameter average (a=b=5.20 Å, c=11.17Å) with Z=2[12].
The properties of these double tungstates depend strongly on their morphology and the distribution of alkanes and the size of the trivalent elements. In this work, we have substituted the trivalent cation Gd^{3+} in $LiGd(WO_4)_2$ by activator ions: europium (Eu^{3+}), erbium (Er^{3+}) and thulium (Tm^{3+}), because their ionic radii and charge valance are similar. First we have grown $LiGd_{0.98}RE_{0.02}(WO_4)_2$ single crystal fibers where RE = Eu, Er and Tm by (µPD) technique, with pulling rate equal to 0.15 mm min^{-1} and meniscus height around 200 µm, in another hand we have shown emission transitions by Photoluminescence spectra, in order to observe

behaviors of theses ions in LiGd $(WO_4)_2$ fiber crystal host, and verify the effects of disorder structure in the doped host. This will be helpful to perform a light phosphor and emission laser.The absorption transitions for the thulium, europium, and erbium were evaluated through absorption spectrum.The emission transitions correspond to $^1G_4 \rightarrow {}^3F_4$, $^3F_2 \rightarrow {}^3H_6$, $^3F_3 \rightarrow {}^3H_6$, $^3H_4 \rightarrow {}^3H_6$, and $^1G_4 \rightarrow {}^3H_5$ for the thulium, and $^5D_1 \rightarrow {}^7F_2$, $^5D_0 \rightarrow {}^7F_{1\text{-}2\text{-}3\text{-}4}$, for europium, furthermore we found for erbium $^4S_{3/2} \rightarrow {}^4I_{15/2}$, $^2H_{11/2} \rightarrow {}^4I_{15/2}$ transitions in visible and $^4I_{13/2} \rightarrow {}^4I_{15/2}$ in Infrared range which present a good three-level laser, compared to other similar compounds doped only erbium through absorption and emission crosses sections which were evaluated.

We compared with other tungstates, the effect of crystal growth on the surrounding environment of Europium through optical properties characterized by the asymmetry factor of luminescence; $I_{5D0\rightarrow7F2}/I_{5D0\rightarrow7F1}$ (electric dipole transition compared to magnetic dipole transition). The fluorescence lifetime were also performed with a 2 at% RE^{3+}- doped LiGd$(WO_4)_2$. The measured decay curve could be fitted by a single exponential.

Polarized IR and Raman spectra measurements were performed with a 2 at%RE^{3+}- doped LiGd$(WO_4)_2$ to characterize the order-disorder phenomena.

2. Experimental part

Before the crystal growth process, we have synthesized LiGd$(WO_4)_2$ doped 2 at % Er, Eu and Tm single phase through the solid-state reaction. The reactants used were: Li_2CO_3 (Roth 99.999%), WO_3 (Philips, 99.97%), Gd_2O_3 (Philips, 99.99%), Eu_2O_3 (99.99%), Er_2O_3 (99.999%), and Tm_2O_3 (99.999%), of analytical grade purity. They were weighed in stoichiometric molar proportions. Single phases were obtained through the following chemical reaction:

$$Li_2CO_3+(0,98)Gd_2O_3+ 0,02Ln_2O_3+4WO_3 \rightarrow 2LiGd_{0.98}\,Ln_{0,02}(WO_4)_2+CO_2\uparrow$$

Where Ln= Eu, Er and Tm

Singles phases samples were confirmed ~~using~~ by room temperature X-ray diffraction analyses.

Tungstate fibers were grown by the micro-pulling-down method (μ-PD) [16-21]. The growth of LiGd$(WO_4)_2$ doped Europium, Erbium and Thulium singles-crystalline fibers is fast and relatively low-cost compared to bulk crystal growth technique from the melt by Czochralski method. Fibers were grown in air atmosphere at 1115°C by pulling rate 0.08 – 0.15mm/min, in Platinum crucibles, and 100–200 μm of melt meniscus length, with an inner capillary diameter of 0.75 mm and 1 mm length.
in the case of RE-doped LiGd$(WO_4)_2$ fiber growth, it was easier to control the meniscus stability (uniform diameter) by controlling the temperature of the crucible (power). During the crystallization process, a movie through CCD camera of the growth process is recorded to calculate the meniscus length and to follow the growth operation. During all the growth process, the solid/liquid interface was flat with uniform shape(Fig 1).

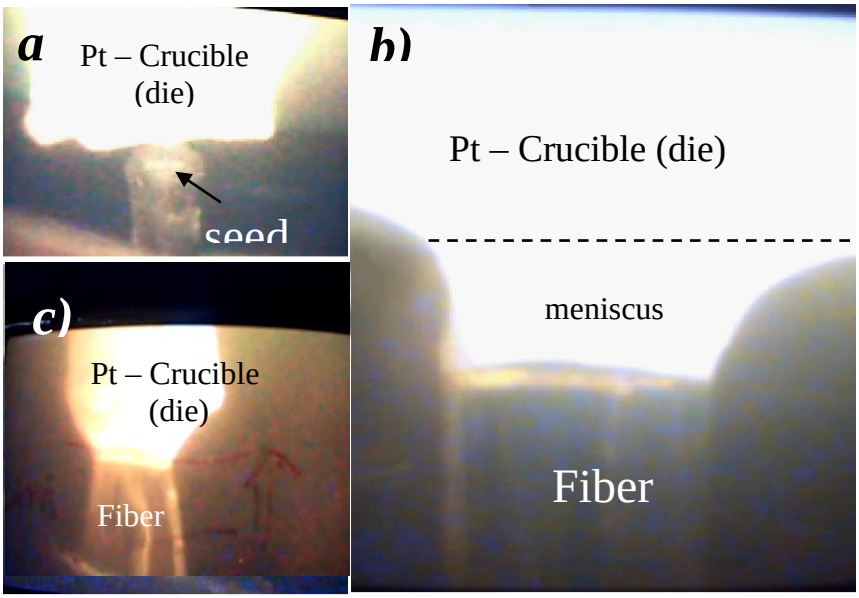

a) Before connection
b) Stationary growth
c) End pulling down

Fig 1. 2 at % Europium- doped LiGd $(WO_4)_2$, fiber pulled by μ-PD technique under stationary stable growth condition

XRD analysis was performed on fibers by a Bruker-AXS D8-Discover diffractometer using Cu Anode Kα radiation (λ = 1.5406 A˚). The data for analyses were obtained in the range of 2θ from 4.5° to 65° recorded with a step size=0.02°.

The grown fibers were cut and polished mechanically, in order to measure the absorption spectra, using a Perkin-Elmer UV–VIS–NIR spectrophotometer (Lambda-35).

The laser excitation used for the visible luminescence analysis was performed with an Ekspla NT342 optical parametric oscillator (OPO) pumped by a pulsed frequency-tripled Nd:YAG laser. The luminescence was collected and transmitted via an optical fiber to an ANDOR SHAMROCK SR303i monochromator equipped with a grating blazed at 500 nm, with a resolution of 0.2 nm using 1200 lines/mm, and analyzed with an iSTAR CCD.

The near infra read emission measurement were performed using excitation with an Analytical Systems dye laser pumped by a frequency-doubled laser with 20mW power. The laser pulse was of 50 μs with 10 Hz repetition rate. In order to compare between spectroscopic results of crystal and powder we carefully took into consideration all optimization conditions, mostly the excitation and the detection conditions to avoid losses such as diffusion, reflection, diffraction. Respecting the mentioned, conditions also ensure the uniformity between the crystal fiber and powder.

The Raman spectra of the fibers crystals were recorded in the range of 100 to 1100cm^{-1} at room temperature using a micro-spectrometer Horiba Jobin-Yvon ARAMIS, equipped with a double monochromator and a spectrograph with holographic lattice at 1800 lines / mm.

The incident beam delivered an excitation source He-Ne laser emitting at 633 nm with a power output of 17 mW, for a spectral resolution of 0.5 cm^{-1} and a spatial resolution of 1 μm with objective x100.

3. Results and discussion

3.1 Crystal growth

We have successfully grown by µ-PD technique single crystalline fibers of $LiGd(WO_4)_2$ doped RE (RE =Eu, Er and Tm). The quality of the fibers are at least equal to the quality $NaGd(WO_4)_2$ (NGW) [22], $NaBi(WO_4)_2$ (NBW) [20], $LiBi(WO_4)_2$ [23] and $LiLa(WO_4)_2$ (LLW) [24]. Crystal fibers are transparent, homogeneous with circular geometry and uniform shape, and have a high optical quality, free from defects such cracks, bubbles and inclusions. Depending on the starting weight charge and the growth parameters, the fibers lengths are from 15 to 50mm and the diameters are between 200µm and 700µm. The transparent crystals fibers are presented in Fig 2. The result of room temperature XRD fibers crystals diagram as a function of the RE element substitution is shown in Fig 3. The peaks were assigned and compared with JCPDF card (04-008-0355), it confirm the $LiGd(WO_4)_2$ single phase. The Fibers crystals belong to the tetragonal system, space group I41/a, unit cell parameters are; a=b= 5.19 Å, c=11.265 Å and the density of the crystal D_c=7.20 g/cm^3, [12, 23].We didn't observed any secondary phases or rare earth free oxides (RE_2O_3) and the fibers don't contain microscopic defects such clusters.

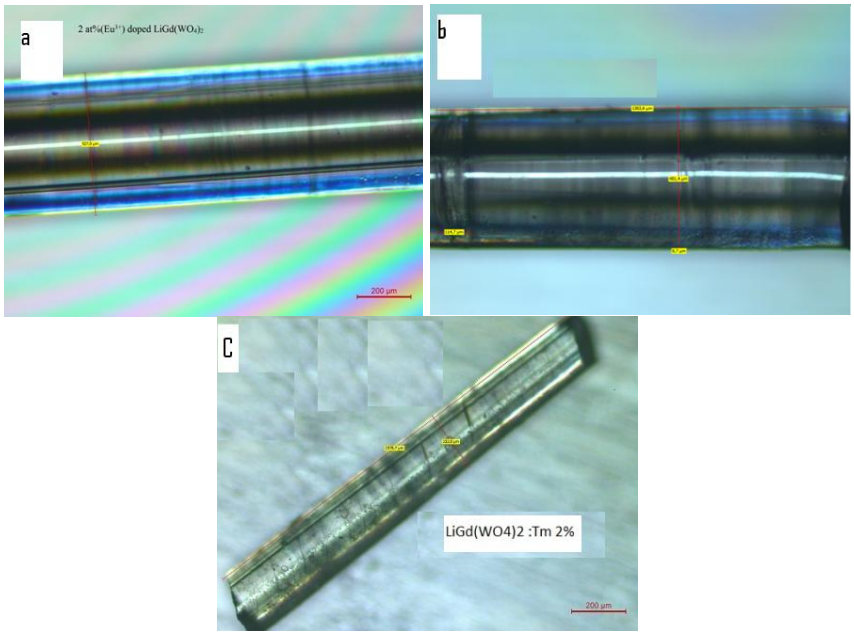

Fig 2. $LiGd_{0.98}RE_{0.02}(WO_4)_2$ fibers grown by µ-PD, (a) RE= Eu, (b) RE= Er, and (c) RE=Tm

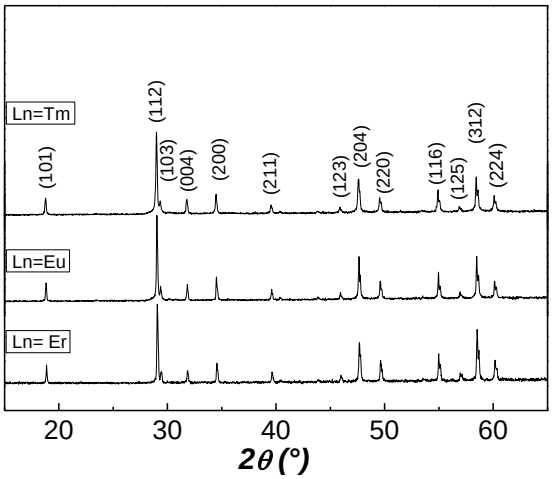

Fig 3. Room temperature X-ray diffraction patterns of 2 at % RE^{3+} doped $LiGd(WO_4)_2$ performed on crashed fibers as a function of activator (RE= Eu, Er and Tm)

The $LiGd_{0.98}Ln_{0.02}(WO_4)_2$ (Ln= Eu, Er and Tm) samples were characterized by Raman and IR spectra measurement at room temperature. The results are similar to the prototype scheelite structure tungstates [12, 25, 26, 27]. The $LiGd(WO_4)_2$ compound crystallizes in structure with the space group I41/a [8]. The polarized IR and Raman spectra parallel and perpendicular to the fibers axis were shown in Fig 4. It is assigned to the vibrational mode frequencies of the Raman and IR spectra in good agreement with scheelite structure.

The isolated tetrahedral $(WO_4)^{-2}$ ion has four fundamental vibrations: the strongest band, $\nu 1$(913 cm^{-1}) for Raman , 915 cm^{-1} for IR corresponding to the symmetric stretching mode of the tetrahedral $(WO_4)^{-2}$. The band registred in 700-850 cm^{-1} range belongs to the asymmetric stretching modes ($\nu 3$).

The observed modes with frequencies 340, and 420 cm^{-1} correspond to the symmetric bending modes; (ν_2) and asymmetric bending (ν_4) of isolated $(WO_4)^{-2}$. The ν_2 band has a higher intensity than ν_4 in Raman spectra and the reverse in IR spectra, and it was confirmed by Miller et al [28].

In the range less than 210 cm^{-1}, the Raman spectrum presents external crystal modes coupled to vibrations of $(WO_4)^{-2}$ tetrahedral and a translational of Li^+ , Gd^{3+} ions at 200 cm^{-1} and 105 cm^{-1} respectively.

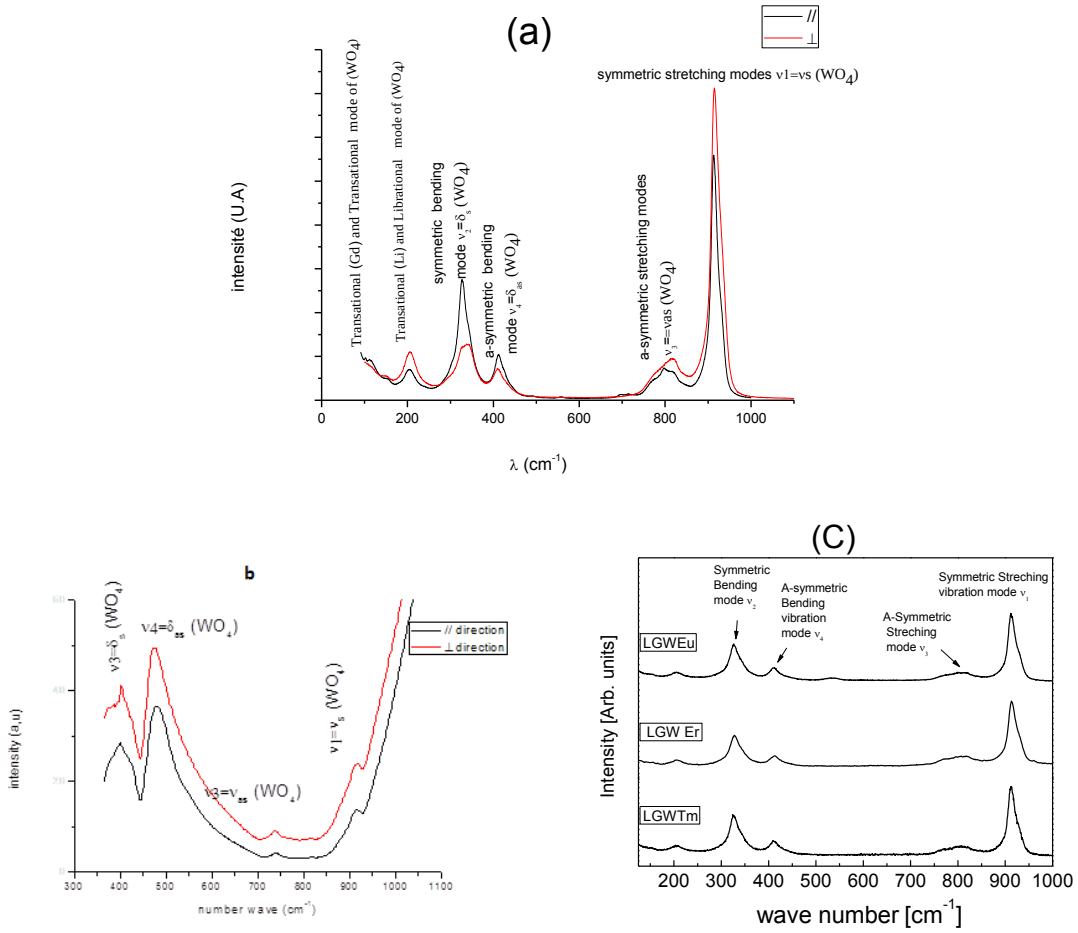

Fig 4. Raman (a) and IR (b) spectra for parallel and perpendicular -polarizations. and effect of RE ion in Raman (c) of $LiGd_{0.98}RE_{0.02}(WO_4)_2$: (LGW RE)

Fig 4.(c) shows that the RE^{3+} rare earth does not affect the modes of the isolated tetrahedral vibration $(WO_4)^{-2}$ because of the low values of these elements (2%) incorporated in the LiGd $(WO_4)_2$ host.

3.2 Absorption characterization

The absorption spectrum of the 2 at %(Ln^{3+}) doped LiGd $(WO_4)_2$ fibers (Ln = Eu, Er , and Tm) at room temperature, are shown in Fig. 5, these spectra provide information on the feasibility of excitation wavelength, and optical pumping relevant to the laser potential of the investigated system.

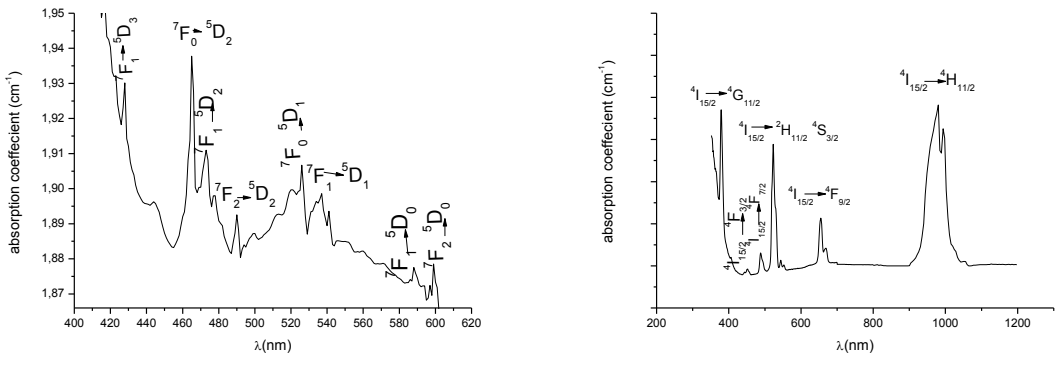

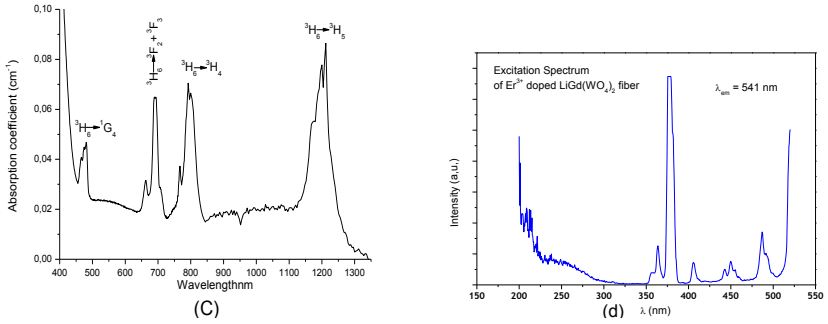

Fig 5. Room-temperature absorption spectrum of crystal. $LiGd_{0.98}RE_{0.02}(WO_4)_2$ crystals fibers (RE= Eu (a), Er (b), Tm (c)) and excitation spectrum for Er at λ_{em}=541nm (d).

Therefore, the absorption cross section was determined by the following equation:

$$\sigma_{abs}(\lambda) = 2.303\, D(\lambda)/d \,/\, N_0 = \alpha(\lambda) / N_0$$

Where **D** (λ) is the optical density at wavelength λ, **d** is the fiber crystal thickness, $\alpha(\lambda)$ is the absorption coefficient at wavelength λ, N_0 is the RE^{3+} doping concentration in $LiGd(WO_4)_2$ fiber crystal with RE = (Er, Tm and Eu) that equals 1,31 $\times 10^{20}$ cm^{-3} for all fibers.

For the Europium dopant the absorption spectrum (fig.5.a) in the range of 400–620 nm presents Eu^{3+} transitions observed in others tungstate hosts. They are shown in Fig.5.a. The absorption bands are attributed to the transitions from the ^7F_j ground state to the $^5D_{0\text{-}1}$ excited states of Eu^{3+} ions. The calculated absorption cross-section is reported, this coefficient does not start from near the zero (the vertical scale starts at 1.85 cm^{-1}), it is related to the small size of the diameter of the fiber (ϕ < 500µm), which the spectrophotometer beam was clipped. The maximum absorption cross section σ_a, in Eu^{3+} ion is attributed to the transition $^7F_0$-$^5D_2$ located in the blue region at 465nm, (σ_a=6.39x10^{-20} cm^2) which is similar to Eu doped $KLu(WO_4)_2$ [29]. These electronic bands can be excited by the blue of the OPO.

Fig. 5.b shows the absorption spectra of 2% at Er^{3+}doped $LiGd(WO_4)_2$ fiber crystal at room temperature in the wavelength range from 350 to 1200 nm. It is similar to Er^{3+}-doped other double tungstates crystals [30]. The Er^{3+} absorption occurs at the wavelength near 378, 451, 489, 521, 543,654, 669 and around 980nm. The absorption cross-section σ_{abs} determined at 489 nm and 520 nm are 10^{-20} cm^2 and 1.55x10^{-20} cm^2 respectively. So, in the near Infrared region, σ_{ab} = 1.65x10^{-20} cm^2 at 980nm. This last one allowed us to use it as a pomping source for IR region.

It can be seen in the excitation spectrum (Fig 5.d) of 2% at Er^{3+}doped $LiGd(WO_4)_2$ that it saturate at the strongest intensity (λ =380 nm), so we are using λ= 489 nm as excitation wavelenght for regarding fluorescence spectrum in the visible.

Fig. 5.D shows the absorption spectra of the 2 at.% Tm^{3+}:$LiGd(WO_4)_2$ fiber crystal. There are five absorption bands sets corresponding to the transitions from the $^3H_6$ ground multiplet to the $^3F_{2\text{-}3}$, $^3H_5$, $^3H_4$, and $^1G_4$ excited multiplets. The absorption cross-section, σ_{abs}, could be obtained for the $^3H_6 \rightarrow {}^3H_4$ transition, which is the main pumping channel. The peak absorptions are at 792 nm and the cross-sections is 4.40×10^{-20}. It is larger than that of tungstate crystals, such as Tm^{3+}:$NaGd(WO_4)_2$ (2.90×10^{-20} cm^2 [31] and Tm^{3+}:$NaLa(WO_4)_2$ 1.39×10^{-20} cm^2 [32]. That is the reason why this fiber crystal is suitable for being laser diode pumped after excitation of $^1G_4$ level at λ= 489nm.

3.3 Photoluminescence characterization

Fig.6, shows the emission spectrum of Er^{3+} doped $LiGd(WO_4)_2$ fiber crystal and powder, corresponding to $^4I_{13/2} \rightarrow {}^4I_{15/2}$ transition in IR domain. The broadening of the emission band is connected to the Stark splitting of $^4I_{13/2}$ and $^4I_{15/2}$ levels. The excitation was performed at 980 nm corresponding to $^4I_{15/2} \rightarrow {}^4I_{11/2}$. It is clear that Er^{3+} doped $LiGd(WO_4)_2$ fiber crystal is more intense in emission than that powder.

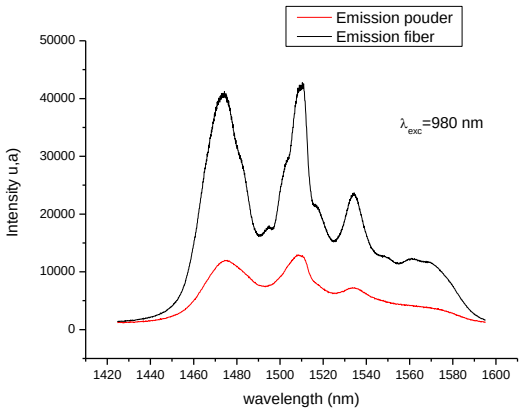

Fig 6. Emission spectra comparison in IR range of 2 at % Er^{3+}-doped $LiGd(WO_4)_2$ grown fiber and powder

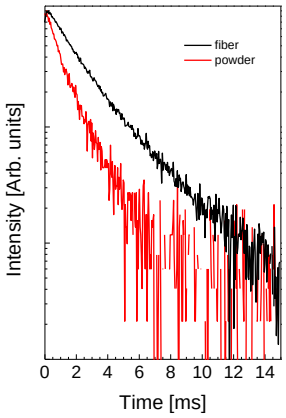

Fig 7. Decay curves of the $^4I_{13/2}$ multiple of the 2 at % Er^{3+}-doped $LiGd(WO_4)_2$ fiber crystal and powder

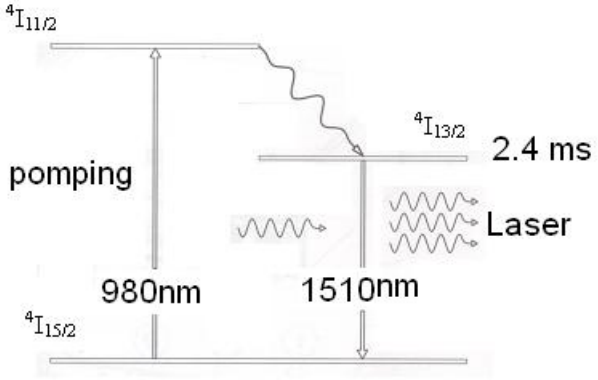

Fig 8. Three-level laser energy diagram for 2 at % Er^{3+}:$LiGd(WO_4)_2$ fiber crystal

The $^4I_{13/2} \rightarrow {}^4I_{15/2}$ transition of Er^{3+} belongs to three-level laser system; It 's clear that the $^4I_{13/2}$, is affected by reabsorption from the ground state absorption or the higher levels like $^4F_{9/2}$, $^4S_{3/2}$ [33 -35]

In order to eliminate the effects of the reabsorption and the radiation trapping corresponding to the resonant transition $^4I_{13/2} \leftrightarrow {}^4I_{15/2}$ of Er^{3+} ion, we carried out ~~our~~ measurements ~~spetially~~ on $LiGd(WO_4)_2$ crystalline fiber at a relatively low dopant concentration of Er^{3+} (2%) [36]

In contrary, for erbium high concentrations, these phenomenon are related with an increase either of the cross-relaxation rate from the $^4I_{9/2}$ level or a population of $^4I_{11/2}$ increases slower , and up conversion rate from this level can be explained by a model presented in [37].

The wide band of the peaks in the absorption and emission spectra ~~measured~~, is due to the tetragonal structure of the scheelite, which is structurally disordered such $LiGd(WO_4)_2$. This disorder could lead, in some cases, to the splitting of the optical lines resulting from a multisite structure due to the 'random occupation by Li and Gd ions. This inhomogeneously

broadened absorption and luminescence bands has been already observed in similar tungstates [24, 36]

In addition, we were able to measure the fluorescence decay times of the $^4I_{13/2}$ multiplet of Er^{3+} doped $LiGd(WO_4)_2$ materials (crystal fiber and powder). The decay pattern for both, can be fitted by a single exponential, We have obtained from the emission decay time of this level τ=2.4 ms and 1.15 ms for fiber and powder respectively (Fig. 7.). So with the same Er^{3+} doped LGW material, we can double the emission lifetime of $^4I_{13/2}$ level if we use a fiber crystal instead of a powder.

Dahua Zhou et al [38] address the experimental methods measuring the $^4I_{13/2}$ multiplet lifetime as on the crystal disk like in $Er:Lu_{1.5}Y_{1.5}Al_5O_{12}$ crystals which the fluorescence lifetime τ_f was fitted to be about 9,9 ms. For this last one, the intrinsic lifetime of the $^4I_{13/2}$ state was lengthened by the radiation trapping process.

For Er^{3+} $LiGd(WO_4)_2$ fiber (present work), it indicate that the decay time value of ~2.4 ms which is slightly lower than that $NaY(WO_4)_2$ which its value ~3.7 ms, [36].

The population of the level $^4I_{11/2}$ should be taken in account when analyzing the decay data of the luminescence of the $^4I_{13/2}$ -> $4I_{15/2}$ transition, which are very critical. If the fluorescence lifetime of the $^4I_{13/2} \rightarrow 4I_{15/2}$ transition of Er^{3+}-doped hosts, is longer than the radiative lifetime, we have a phenomenon of radiation trapping and emission reabsorption, wich may be caused by approach between the decay time of the transition $^4I_{11/2}$->$^4I_{13/2}$ and the lifetime of the $^4I_{13/2}$ level, that leads to repopulation of $4I_{13/2}$ level during its decay which also existed in some other Er^{3+}-doped hosts such as $Er^{3+}:NaGd(WO_4)_2$ [59], $Er^{3+}:NaY(MoO_4)_2$ [60], $Er^{3+}:LiNbO_3$[61], $Er^{3+}:SrWO_4$ [62], $Er^{3+}:KPb_2Cl_5$ [63], $Er^{3+}:KPb_2Br_5$ [64] and $Er^{3+}:LiLa(MoO_4)_2$. [65]. For this last crystal, the fluorescence lifetime of the $^4I_{13/2} \rightarrow {}^4I_{15/2}$ transition was measured to be 7.20 ms, is longer than the radiative lifetime (4.88 ms).
To resolve this problem we can excit the sample directly in the $^4I1_{3/2}$ level or we use the lowest concentration of Er^{3+} dopant.
for certain Er^{3+} doped materials which have low absorption, the emission reabsorption $^4I_{15/2} \rightarrow {}^4I_{13/2}$, is negligible [66]

To get the highest efficiency of lasing by the $^4I_{13/2} \rightarrow {}^4I_{15/2}$ transition under pumping ~~to~~ the $^4I_{11/2}$ level, we have used powder of thin thickness (0.5mm) pressed at 4000 kg/cm^2.

One of the solutions to avoid Radiation trapping effect, is the use of a pinhole method discriped by a theorical model [39-40].

Fig.8 presents three-level laser energy diagram for 2 at % $Er^{3+}:LiGd(WO_4)_2$fiber crystal in infrared region .

The efficiency of such laser is related to the ratio of the absorption coefficients at the pump and laser emission wavelength: $\frac{\alpha(\lambda_p)}{\alpha(\lambda_L)} = \frac{\sigma_{ab}(\lambda_p)}{\sigma_{ab}(\lambda_L)}$

This ratio is set for a given matrix. Nevertheless, it is possible to increase this ratio by codoping the matrix with another rare earth ion, having a resonant transition of erbium, favoring the energy transfer of this ion towards erbium -up conversion- : this is the case of the ytterbium ion as sensitizer as the case of the most matrices [41], and as it is possible to have this ratio higher than unit ; if the absorption cross-section at pumping wavelength is high as our work , Er^{3+}doped LiGd $(WO_4)_2$ single crystal compound having high absorption cross sections around the wavelength of the pump λ= 980 nm, $\sigma_{ab} = 1.65x10^{-20}$ cm^2 , is higher than that of an Er doped garnet compound such that YAG or LuAG. In fact, the tungstates have very high absorption cross-sections [36].
Dahua Zhou et al, used 980 nm wavelenght as the excitation source presented in (Er doped LuYAG). Despite the fact that the absorption cross-section at this wavelength is weak [38].

Fig.9, show the emission spectrum of 2 at % Er^{3+} doped $LiGd(WO_4)_2$ in visible spectral range after excitation at 489 nm. We have observed the two mains emissions in the green. The emission in the 525 to 535 nm range is assigned to the $^2H_{11/2} \rightarrow {}^4I_{15/2}$ transition, and the emission in the 537 to 558 nm range corresponding to the $^4S_{3/2} \rightarrow {}^4I_{15/2}$ transition. This spectrum is similar to the spectrum obtain previously on powder [42].

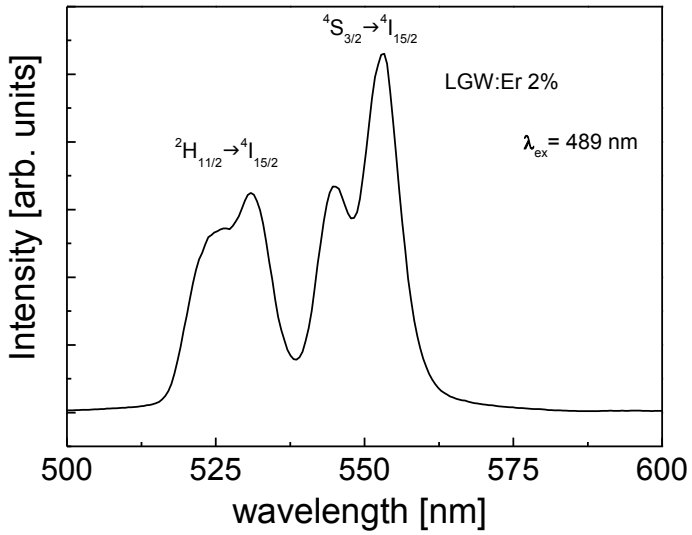

Figure 9. Emission spectra in visible domain of 2 at % Er^{3+}- doped $LiGd(WO_4)_2$ grown fiber

Fig. 10 show the luminescence decay of Er^{3+}- doped $LiGd(WO_4)_2$ fiber and powder of the $^2H_{11/2}$ level after excitation at 489 nm and record at 553 nm. The lifetime was evaluated by fitting of a single exponential on the decay. The emission lifetime was found at 17µs and 18 µs for the powder and the crystal fiber respectively. The lifetime obtained on the powder is in good agreement with precedent results obtained in [42] on the same material. For the single crystal fiber this result is comparable to the crystal of similar compound, $NaGd(WO_4)_2$ crystal (τ_{em}= 26µs) [43], and $KGd(WO_4)_2$ single crystals (τ_{em}= 27µs) [44].

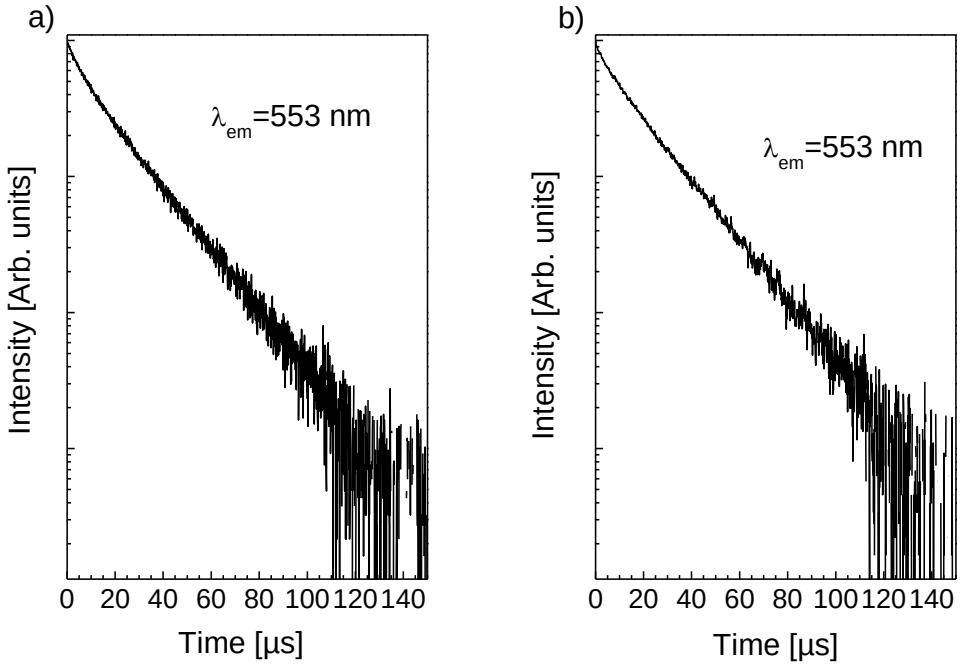

Fig 10. Room temperature fluorescence decay curves of the $^2H_{11/2}$ level of the 2% Er^{3+}-doped $LiGd(WO_4)_2$ crystal: a) powder and b) fiber.

The emission spectrum of the 2 at %Tm^{3+}: LiGd $(WO_4)_2$ fiber is shown in Fig.11. The spectrum present emissions peaks at 650, 675, 802 and 840 nm corresponding to the $^1G_4 \rightarrow {}^3F_4$, $^3F_3 \rightarrow {}^3H_6$, $^3H_4 \rightarrow {}^3H_6$, and $^1G_4 \rightarrow {}^3H_5$ transitions respectively of Tm^{3+} . This provides a better agreement with others spectroscopic results [45].

The fluorescence decays of 2 at % Tm^{3+} LiGd $(WO_4)_2$ fiber crystal of the $^1G_4$, $^3H_4$, levels emitting was measured and presented in Fig.12. The emissions lifetimes were estimated to 40 and 113 μs for $^1G_4$, $^3H_4$, levels respectively by the fitting with a single exponential.
The non-exponential character of the decays corresponding to a relatively high dopant concentration can be described by the model developed by Inokuti and Hirayama [46].
This difference in value is due to the cross relaxations between Tm^{3+} ions, for the $^1G_4$ multiplet which are stronger than that for the $^3H_4$ multiplet, because the energy gap between the $^1G_4$ and the next lower $^3F_2$ multiplets is more important than the maximum phonon energy of the $[WO_4]_2^-$ group [47]. These values of the decays are closed to the Tm^{3+}-doped $LiLa(MoO_4)_2$ of the same structure, they were derived to be 51 and 105μs, respectively of the $^1G_4$ and $^3H_4$ multiplets. It is identified to be isostructural to $CaWO_4$ (scheelite) with space group I41/a (C_{4h}), and same lattice parameters with LGW crystal [48].

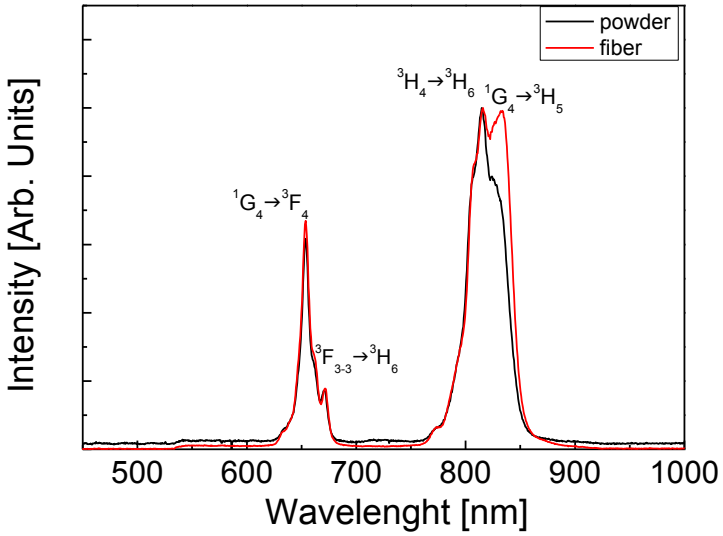

Fig 11. Emission spectra of Tm^{3+} doped $LiGd(WO_4)_2$ grown fiber and powder

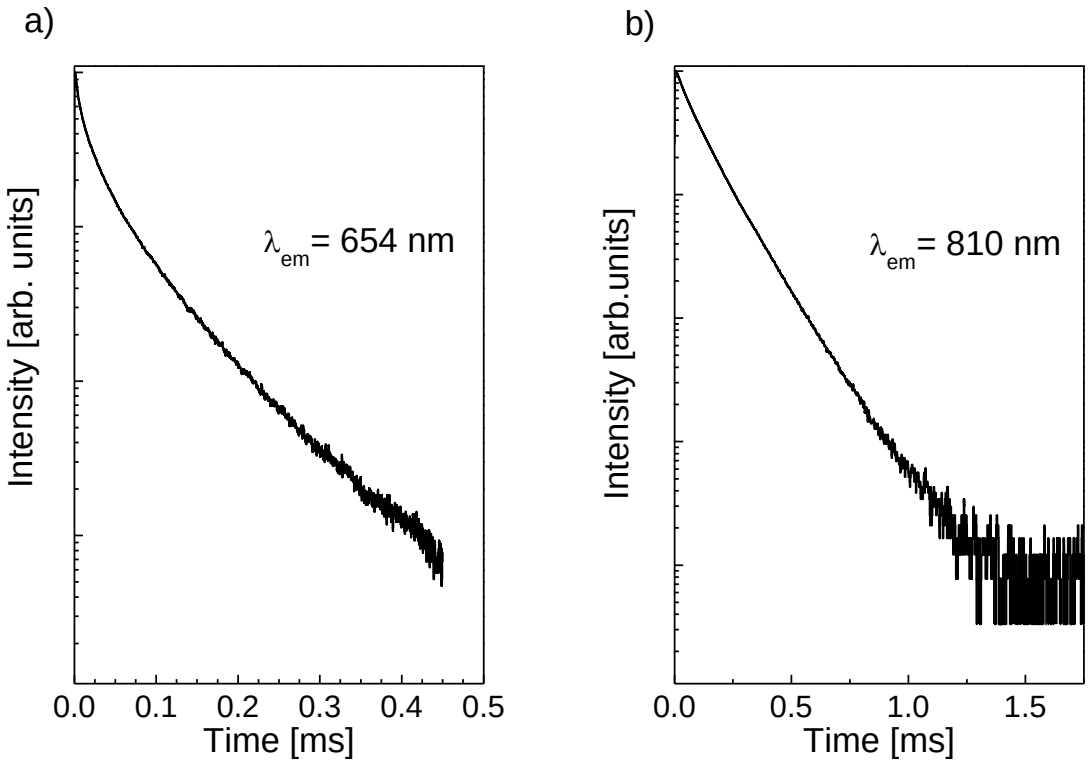

Fig 12. Room temperature fluorescence decay curves ,(a) $^1G_4$ and (b) $^3H_4$ level of the 2% Tm^{3+}:$LiGd(WO_4)_2$ crystal.

Fig. 13 (a) shows the emission spectra as function of the excitation wavelength for the 2 at % doped Eu^{3+}:LGW fiber crystal. The spectra show $^5D_{0-1} \rightarrow ^7F_{0-1-2-3-4}$ transitions of the europium. As we increase the wavelength of excitation, the intensity of the emission peaks from $^5D_1$ level decrease. It is also possible to separate the $^5D_0 \rightarrow ^7F_{0-1-2-3-4}$ and $^5D_1 \rightarrow ^7F_{0-1-2\ -3-4}$

emissions by time resolver spectroscopy (Fig.13b). Between 250 ns to 5 µs the emissions of the $^5D_1$ are preeminent, and the emission of the $^5D_0$ are the main ones after 100 µs.
Those emissions spectra are similar to the spectra of the Eu^{3+} ion in other tungstate hosts [49-51]. It presents the main emission peak at 613 nm, corresponding to the electric dipole; $^5D_0 \rightarrow ^7F_2$ transition of Eu^{3+}. Three weak peaks at 590, 652 and 697 nm are attributed to the $^5D_0 \rightarrow ^7F_1$, $^5D_0 \rightarrow ^7F_3$ and $^5D_0 \rightarrow ^7F_4$ transitions of Eu^{3+} respectively. By intensity comparison between the different transitions, we can studies the influence of Eu^{3+} site symmetry in $LiGd(WO_4)_2$ fiber crystal. The dominance of $^5D_0 \rightarrow ^7F_2$ in the emission spectrum confirms the presence of low symmetry site of Eu^{3+} located in this fiber. The electric dipole corresponding to the $^5D_0 \rightarrow ^7F_2$ transition which it dominates in sites without inversion symmetry non – centrosymmetric - is more efficient than the magnetic dipole, corresponding to the $^5D_0 \rightarrow ^7F_1$ transition dominates in sites with inversion symmetry.

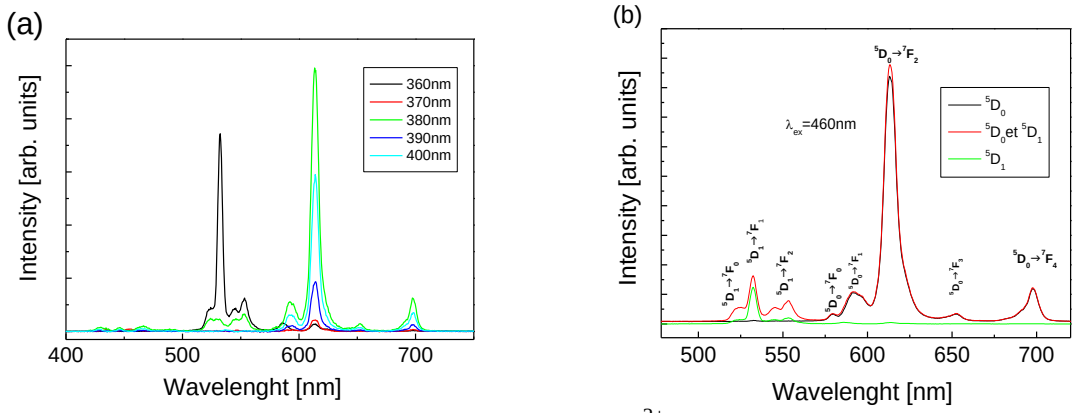

Fig 13. Emission spectra in the visible domain of Eu^{3+}-doped $LiGd(WO_4)_2$ grown fiber (a) as a function of excitation wavelength (b) and time resolved spectroscopy.

In order to attempt an understanding of the emission spectrum measure, as shown in Fig. 14, we have proposed an energy level diagram scheme.

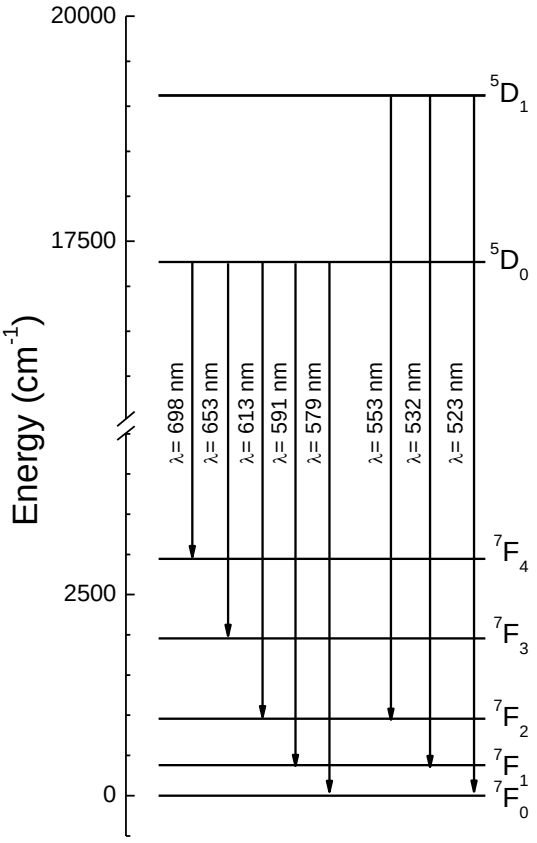

Fig 14. Energy diagram of Eu^{3+} emission in $LiGd(WO_4)_2$ fiber crystal from $^5D_0$ and $^5D_1$ multiples

Eu^{3+} doped $LiGd(WO_4)_2$ fiber crystal substitute Gd^{3+} in (C_2) site symmetry, it's emission is dependent on the local crystal field environment. Because the $^5D_0 \rightarrow {}^7F_2$ transition intensity is larger than that of the $^5D_0 \rightarrow {}^7F_1$, we can calculate the asymmetry parameter (R) called asymmetry factor of luminescence, which is the ratio of the integral intensities; $I_{5D0\rightarrow 7F2}/I_{5D0\rightarrow 7F1}$. It is a good measure for the symmetry of the Eu^{3+}. In our fiber crystal it is around 9, this value is similar to that of Eu^{3+}:$LiLa(WO_4)_2$ fiber crystal grown by µ-pulling down [24]. It is higher than Eu^{3+}:$KLu(WO_4)_2$, and Eu^{3+}:$KYb(WO_4)_2$ single crystal, which are around 3 and 4 respectively [52-29-53]. This indicates a widely difference in bonds distortion in the coordination of the europium site. It is related to the short average distance between the Eu–O. In the case of Eu^{3+}:$KY(WO_4)_2$ the asymmetry R parameter is larger than our fiber crystal, the value equal to 10-12 [50]. The increasing of the R parameter can be explained by the difference in the ionic radii of Eu^{3+} (1.066 Å), Gd^{3+} (1.053 Å) which is smaller than between Eu^{3+} (1.066 Å), and Y^{3+}(1.019 Å). The environment of deformed squared antiprisms LiO_8 and GdO_8 has a greater distortion in $LiGd(WO_4)_2$ than the LuO_8 polyhedron in monoclinic $KLu(WO_4)_2$. This is produced by the covalence of the Eu-O bond, and the strong crystal field around Eu^{3+} ion. The emission from the $^5L_6$ and $^5D_3$ levels of $LiEu(WO_4)_2$ fiber using excitation at 395 nm, has been presented by Jair Ricardo de Moraes et al [24]. These levels do not effect the local environment of the deformed squared antiprisms LiO_8 and GdO_8, on the other hand, the compound $LiEu(WO_4)_2$ does not contain the GdO_8 polyhedral which we studied in this work. Moreover, a quenching is observed in $LiEu(WO_4)_2$ fiber using excitation

at 395 nm (see reference Number We studied the emission lifetime of 2 at % Eu^{3+} $LiGd(WO_4)_2$ fiber crystal of the europium emission $^5D_0 \rightarrow {}^7F_2$ transition at 613 nm by exciting the sample at 460 nm (Fig1 4), it's about 467 μs better than Eu^{3+} $KY(WO_4)_2$ crystal [29] and Eu^{3+} $Pb(WO_4)$ [54].

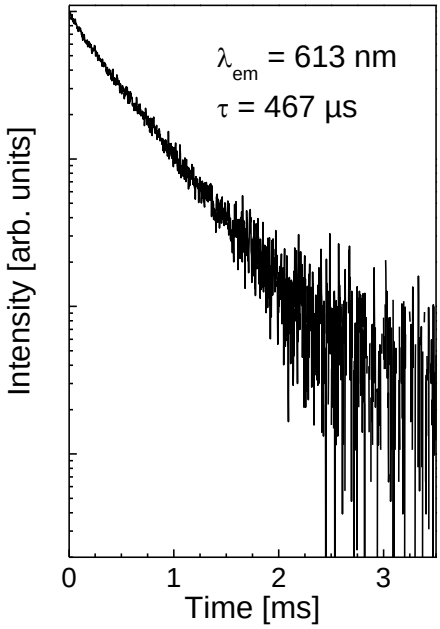

Fig 15. Room temperature fluorescence decay curves of the $^5D_0 \rightarrow {}^7F_2$ multiplet of the 2% Eu^{3+}:$LiGd(WO_4)_2$ crystal.

The emission cross-section σ_{em}, (λ) of 2 at % Eu, Er and Tm-doped $LiGd(WO_4)_2$ can be calculated by the Fuchtbauer–Ladenburg (F–L) formula : [55]

$$\sigma_{em}(\lambda) = \frac{\lambda^5}{8\pi n^2 c\ \tau_r} \frac{I(\lambda)}{\int \lambda I(\lambda) d\lambda}$$

where **I(λ)** is the measured fluorescence intensity at wavelength **λ,** and τ_r is the spontaneous emission probability of the hgier transition of eatch spectra, **n** is the refractive index (2.07 for $LiGd(WO_4)_2$), and **c** is the speed of light.

The obtained emission cross-sections σ_{em} are shown in Fig 16 , for $LiGd_{(0.98)}Ln_{0.02}(WO_4)_2$ (Ln= Eu, Er and Tm)

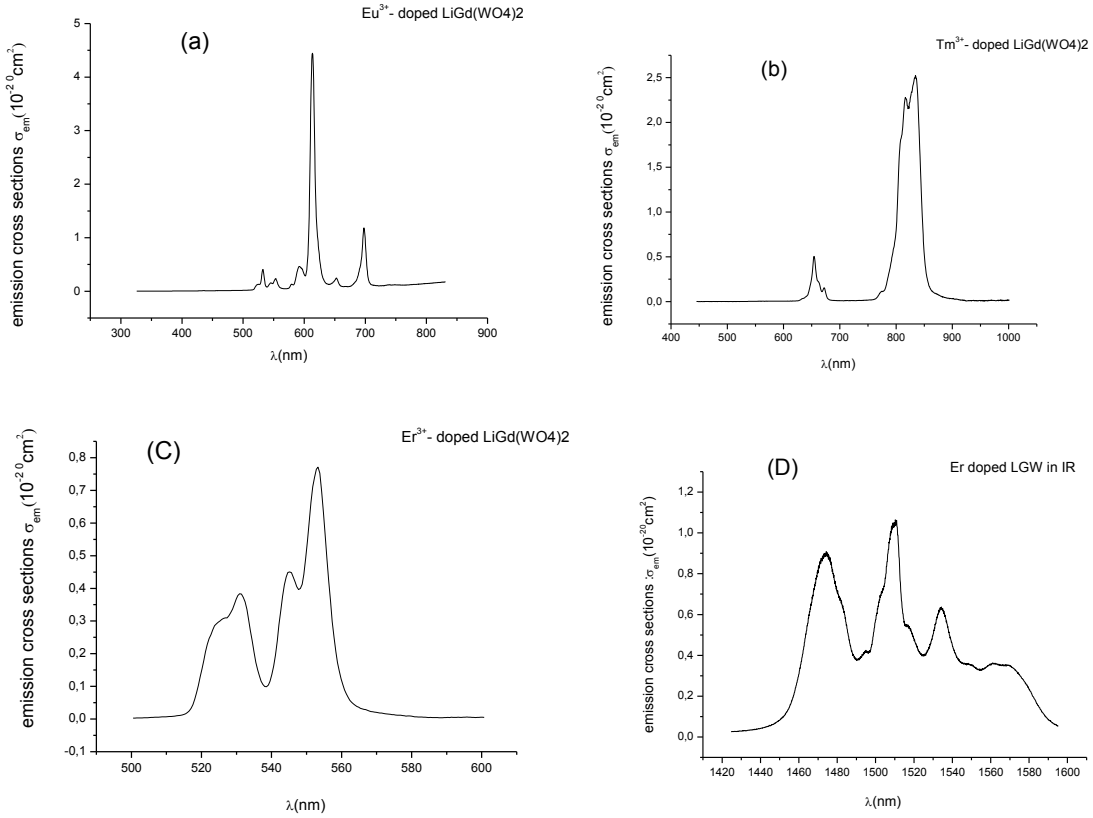

Fig 16. Emission cross section in visible region of 2 at % Ln :LiGd(WO4)2 crystal with Ln = Eu (a) , Tm (b), Er (c) and Er in IR region (d)

The measured life time and the calculated emission cross-sections of Ln^{3+}:$LiGd(WO_4)_2$ (Ln=Eu, Er and Tm) crystals are presented in Table1. In our case the Er^{3+} doped $LiGd(WO_4)_2$ have a good emission cross-sections compared to others crystals materials such as doped-Er^{3+}:$NaGd(WO_4)_2$ and codoped Er^{3+}/Yb^{3+}:$NaY(WO_4)_2$.

Table 1
The electron transitions ,measured lifetimes, and emission cross-section of Ln^{3+}:$LiGd(WO_4)_2$ (Ln=Eu, Er and Tm) crystal compared to others crystals

Elaborated Samples	**electron Transitions**	**σ_{em} (10^{-20} cm^2)**	**Wave length (nm)**	**τ_{rd} (ms**	**Ref**
Eu^{3+}:$LiGd(WO_4)_2$	$^5D_0 \rightarrow {}^7F_0$	0.133	579		
	$^5D_0 \rightarrow {}^7F_1$	0.46	591		
	$^5D_0 \rightarrow {}^7F_2$	4.44	613	0.467	This work
	$^5D_0 \rightarrow {}^7F_3$	0.247	653		
	$^5D_0 \rightarrow {}^7F_4$	1.18	698		
	$^5D_1 \rightarrow {}^7F_1$	0.40	532		
	$^5D_1 \rightarrow {}^7F_2$	0.23	553		

Tm^{3+}:$LiGd(WO_4)_2$	$^1G_4 \rightarrow {}^3F_4$, $^3F_{2\text{-}3} \rightarrow {}^3H_6$ $^3H_4 \rightarrow {}^3H_6$ $^1G_4 \rightarrow {}^3H_5$	0.504 0.153 0.115 2.28 2.52	650 675 775 810 834	0.040 0.113 	 This work
Er^{3+}:$LiGd(WO_4)_2$	$^2H_{11/2} \rightarrow {}^4I_{15/2}$ $^4S_{3/2} \rightarrow {}^4I_{15/2}$	0.45 0.77	545 553	 0.018	 This work
Er^{3+}:$LiGd(WO_4)_2$ Er^{3+}:$NaGd(WO_4)_2$ Er^{3+}:$NaBi(WO_4)_2$ Er^{3+}:$NaY(WO_4)_2$ Er^{3+}/Yb^{3+}:$NaY(WO_4)_2$	$^4I_{13/2} \rightarrow {}^4I_{15/2}$	1.063 0.637 0.78 0.02	1510 1534 ~1530 1530 1530 1530	2.4 3.8 3.2 4.59 4.19	This work 56 57 58 41

4. Conclusion

A series of single crystals fibers 2% RE^{3+}:$LiGd(WO_4)_2$ (RE=Tm, Er and Eu) were successfully grown by µ-PD technique after elaboration of single phases by the conventional solid-state reaction method. The obtained single crystal fibers were about 0.2–0.6 mm in diameter and with average of 10-20 mm length. The obtained crystals transparency quality is high and they are very promising for fibers optical applications. The LGW: Tm^{3+}, LGW: $Er^{3+}$and LGW: Eu^{3+} phosphors show the absorption and emissions characteristics of Tm^{3+}, Er^{3+}, and Eu^{3+} respectively, The absorption and emission cross-section of the $^4I_{15/2} \rightarrow {}^4I_{11/2}$ and $^4I_{13/2} \rightarrow {}^4I_{15/2}$ transition are 1.65×10^{-20} cm^2 and 1.063×10^{-20} m^2, respectively. The lifetime of this last state was arround 2.40 ms. These spectroscopic parameters allow the comparison of our material with other Er^{3+}-doped materials (see Table 1)

Relaying on the infomtions provided by the electronic dipole and magnetic dipole transitions $^5D_0$ to the $^7F_2$,and $^5D_0$ to the $^7F_1$, the calculated I_{613}/I_{591} ratio for LGW: Eu^{3+} presents an excellent structural probe for investigating the local environment of the deformed squared antiprisms LiO_8 and GdO_8 which have a greater distortion in the $LiGd(WO_4)_2$ host lattice.

In addition, decay times of the emitting state in the visible region for fibers crystal LGW: Er^{3+}, LGW: Eu^{3+}, LGW: Tm^{3+} present a good luminescence efficiency compared to other known double tungstates powder.

Reference

[1] A.M. Kaczmarek and R. Van Deun, Chemical Society Reviews, 2013, 42, 8835-8848

[2] S. Dutta, S. Som, J. Priya and S. Sharma, Solid State Sciences, 2013, 18, 114-122.

[3] L. You, Y. Cao, Y. Sun, P. Sun, T. Zhang, Y. Du and G. Lu, Sensors and Actuators B: Chemical, 2012, 161, 799-804

[4] B. Karami, S. Khodabakhshi and Z. Haghighijou, Chemical Papers, 2012, 66, 684-690

[5] V. Petrov, M. C. Pujol, X. Mateos, O. Silvestre, S. Rivier, M. Aguiló, R. M. Solé, J. Liu, U. Griebner and F.Díaz, Laser & Photon. Rev. 1, (2007)179–212

[6] M. Derbal, Djamel Ouadjaout, F. Siserir, Véronique Jubera, Jean-Pierre Chaminade, Alain Garcia, Oudomsack Viraphong ,M. Kadi Hannifi, Optical Materials 32, 7 (2010) 756-758

[7] A. García-Cortés, J. M. Cano-Torres, M. D. Serrano, C. Cascales, C. Zaldo, S. Rivier, X. Mateos, U.Griebner and V. Petrov IEEE J. Quantum Electron. 43, (2007)758-764

[8] J. Liu, J. M. Cano-Torres, F. Esteban-Betegón, M. D. Serrano, C. Cascales, C. Zaldo, M. Rico, U. Griebner and V. Petrov, Opt. Laser Technol. 39, (2007)558-561

[9] C. Cascales, M. D. Serrano, F. Esteban-Betegón, C. Zaldo, R. Peters, K. Petermann, G. Huber, L. Ackermann, D. Rytz, C. Dupré, M. Rico, J. Liu, U. Griebner and V. Petrov,Phys. Rev. B 74, (2007)174114:1-15
[10]. A. García-Cortés, J. M. Cano-Torres, X. Han, C. Cascales, C. Zaldo, X. Mateos, S. Rivier, U. Griebner, V.Petrov and F. J. Valle, J. Applied. Phys. 101, 0(2007).63110:1-7.
[11]. M. Rico, U. Griebner, V. Petrov, P. Ortega, X. Han, C. Cascales and C. Zaldo, J. Opt. Soc. Am. B 23, (2006)1083-1090
[12]. B. Rekik , M. Derbal , L. Guerbous , D. Oudjaout , A. Nehari , E. Romeo , A. Brenier , A. Yoshikawa ,K. Lebbou,Optical Materials, Volume 33 (2011) 1638-1642
[13] P. Parhi, T. Karthik and V. Manivannan, Journal of Alloys and Compounds, 2008,465, 380-386
[14]. X. Liu, W. Hou, X. Yang and J. Liang, Cryst Eng Comm, 2014, 16, 1268-1276.
[15]. G. Benoît, J. Véronique, A. Arnaud and G. Alain, Solid State Sciences, 2011, 13, 460-467.
[16].D.-H. Yoon and T. Fukuda. Journal of Crystal Growth, 144:201–206, 1994
[17].T. Fukuda, p. Rudolph, s. Uda, book on fiber crystal growth from the melt (springer, berlin 2004).
[18].A. García-Cortés, C. Zaldo, C. Cascales, X. Mateos, and V. Petrov , Optics Express, Vol. 15, (2007) 18162-18167
[19].D.H. Yoon, T. Fukuda, J. Korean, Assoc. Cryst. Growth 4 (1994) 405
[20].A. Karek , K. Lebbou , M. Diafa, A. Brenier, G. Boulon, J of Materials research Bulletin 42 (2007)532-543
[21] J.Hanuza, M. Maczka, and J. H. vader Maas , J of solide state and chemistry 117, 177-188 (1995)
[22] Y. Terada, K. Shimamura, T. Fukuda, J. Alloys Comp. 275-277 (1998) 697.
[23] B. Rekik a,n, M. Derbal a, K. Lebbou b, M.E.A. Benammar, J. Crystal Growth 101-104 (2016) 452
[24] Jair Ricardo de Moraes, Sonia Licia Baldochi, Leonardo dos Reis Leano Soares, Vera Lucia Mazzocchi, Carlos Benedicto Ramos Parente, Lilia Coronato Courrol, Materials Research Bulletin 47 (2012) 744–749
[25] G. Benoît, J. Véronique, A. Arnaud and G. Alain, Solid State Sciences, 2011, 13, 460-467
[26] B. Rekik, M.Derbal, O.Benamara, K.Lebbou Journal of crystal Growth 405(2014)11–15
[27] S. P. S. Porto and J. F. Scott, Phys. Rev., 157, No. 3, 716-719 (1967).
[28] A. Miller, E. J. Baran, and R.O. Carter, Structure Bonding 26, 81 (1976), and references therein.
[29] M.C. Pujol n, J.J.Carvajal, X.Mateos,R.Sole, J.Massons,M.Aguilo´, F.Dı´az Journal of Luminescence 138 (2013) 77–82
[30] M. Rico, U. Griebner, V. Petrov, P. Ortega, X.M. Han, C. Conceptión, et al., J. Opt. Soc. Am. B 23 (2006) 1083.
[31] J.M. Cano-Torres, M.D. Serrano, C. Zaldo, M. Rico, X. Mateos, J.H. Liu, U. Griebner, V. Petrov, F.J. Valle, M. Galan, G. Viera, J. Opt. Soc. Am. B 23 (2006) 2494–2502.
[32] J.M. Cano-Torres, X. Han, A. Garcia-Cortes, M.D. Serrano, C. Zaldo, F.J. Valle, X. Mateos, S. Rivier, U. Griebner, V. Petrov, Mater. Sci. Eng. B 146 (2008) 22–28..
[33] M. Rico, A. Méndez-Blas, V. Volkov, M.Á. Monge, C. Cascales, C. Zaldo, et al., J. Opt. Soc. Am. B 23 (2006) 2066.
[34] K.A. Subbotin, E.V. Zharikov, V.A. Smirnov, Opt. Spectrosc. 92 (2002) 601.
[35] D.S. Sumida, T.Y. Fan, Opt. Lett. 19 (1994) 1343.

[36] V. Fromzela, N. Ter-Gabrielyana, M. D. Serranob, D. E. Laherab, C. Cascalesb , C. Zaldob, M. Dubinskiia, Lasers, Sources, and Related Photonic Devices Technical Digest © 2012 OSA
[37] T. Jensen, A. Diening, G. Huber, and B. H. T. Chai, Opt. Lett. 21, 585 (1996)..
[38] Dahua Zhou,1 Xiaodong Xu,2,* Changtai Xia,1 Deyuan Shen,3 Shishu Cheng,1 Dongzhen Li,1 Juqing Di,1 Zhiwei Zhao,1 Feng Wu,2 and Jun Xu2 Vol. 28, No. 10 / October 2011 / J. Opt. Soc. Am. B
[39] Eichhorn, M. (2009). Fluorescence reabsorption and its effects on the local effective excitation lifetime. Applied Physics B, 96(2-3), 369.
[40] KÜHN, Henning, et al. Model for the calculation of radiation trapping and description of the pinhole method. Optics letters, 2007, 32.13: 1908-1910.
[41] Z.X. Cheng, S.J. Zhang, F. Song, H.C. Guo, J.R. Han, H.C. Chen, J. Phys. Chem. Solids 63 (2002) 2011.
[42] A. Demiaï, M. Derbal, L. Guerbous, B. Rekik, Optical Materials 65 (2016) 137-141
[43] H. Huang, X.H. Gong, Y.J. Chen, Y.F. Lin, J.S. Liao, X.Y. Chen, Z.D. Luo,Y.D. Huang, Appl. Phys. B 89 (2007) 73.
[44] M.C. Pujol, M. Rico, C. Zaldo, R. So le, V. Nikolov, X. Solans, M. Aguilo, F. Dıaz, Appl. Phys. B 68 (1999) 187.
[45] Yang Zhang, Weitao Gong, Jingjie Yu, Yuan Lin,a Guiling Ning, J. RSC advences 2015
[46] M. Inokuti, F. Hirayama, J. Chem. Phys. 43, 1978 (1965)
[47] J. Hanuza, M. M ¸aczka, J.H. van der Maas, J. Mol. Struct. 348 (1995) 349‑352
[48] Y.W. Wei, Y.J. Chena, Y.F. Lin, X.H. Gong, Z.D. Luo, Y.D. Huang, Journal of Alloys and Compounds 484 (2009) 529-534
[49] L.G. van Uitert, in: P. Goldenberg (Ed.), Luminescence of Inorganic Solids, Academic Press, New York, 1966, pp. 465–539.
[50] J.P.M. van Vliet, G. Blasse, L.H. Brixner, J. Solid State Chem. 76 (1988) 160–166.
[51] C.A. Kodaira, H.F. Brito, M.C.F.C. Felinto, J. Solid State Chem. 171 (2003) 401–407.
[52] P.A Loiko and Al, Journal of luminescence 153 (2014) 221-226
[53] M. Galceran, M.C. Pujol, P. Gluchowski , W. Stre¸k, J.J. Carvajal, X. Mateos, M. Aguilo, F. Diaz. 32 (2010) 1493–1500
[54] O. Chukova, S. Nedilko, V. Scherbatskyi, J. Lumin. 130 (2010) 1805–1812
[55] D.E. McCumber, Phys. Rev. 136 (1964) A954. B.F. Aull, H.P. Jenseen, IEEE J. Quantum Elect. 18 (1982) 925.
[56] J.H. Huang, X.H. Gong, Y.J. Chen, Y.F. Lin, J.S. Liao, X.Y. Chen, et al., Appl. Phys. B 89 (2007) 73.
[57] M. Rico, A. Méndez-Blas, V. Volkov, M.Á. Monge, C. Cascales, C. Zaldo, et al., J. Opt. Soc. Am. B 23 (2006) 2066.
[58] F. Song, H. Tan, M.R. Shang, G.Y. Zhang, Z.X. Chen, H.C. Chen, Acta Phys. Sinica 51 (2002) 2375.
[59]J.H. Huang, X.H. Gong, Y.J. Chen, Y.F. Lin, Q.G. Tan, Z.D. Luo, et al., Mater. Lett. 61 (2007) 3400.
[60]X.Z. Li, Z.B. Lin, L.Z. Zhang, G.F.Wang, J. Cryst. Growth 293 (2006) 157.
[61] J. Amin, B. Dussardier, T. Schweizer, M. Hempstead, J. Lumin. 69 (1996) 17.
[62] G.H. Jia, C.Y. Tu, J.F. Li, X.A. Lu, Z.Y. You, Z.J. Zhu, B.C.Wu, J. Appl. Phys. 98 (2005) 093525.
[63] N.W. Jenkins, S.R. Bowman, S.O. Connor, S.K. Searles, J. Ganem, Opt. Mater. 22 (2003) 311.
[64] U. Hommerich, E.E. Nyein, S.B. Trivedi, J. Lumin. 113 (2005) 100.
[65] Xinyang Huanga,b,*, GuofuWangb Journal of Alloys and Compounds xxx (2008) xxx–xxx

[66]Mauricio Rico, Antonio Méndez-Blas, Vladimir Volkov, María Ángeles Monge, Concepción Cascales, and Carlos Zaldo /J. Opt. Soc. Am. B / Vol. 23, No. 10/October 2006